Applied Catalysis B: Environmental 87 (2009) 30–36

Contents lists available at ScienceDirect

Applied Catalysis B: Environmental

journal homepage: www.elsevier.com/locate/apcatb

Photoassisted degradation of endocrine disruptors over CuO_x–FeOOH with H_2O_2 at neutral pH

Yulun Nie, Chun Hu *, Jiuhui Qu *, Xu Zhao

State Key Laboratory of Environmental Aquatic Chemistry, Research Center for Eco-Environmental Sciences, Chinese Academy of Sciences, Beijing 100085, China

ARTICLE INFO

Article history:
Received 3 March 2008
Received in revised form 19 August 2008
Accepted 22 August 2008
Available online 31 August 2008

Keywords:
Endocrine disruptors
CuO_x
FeOOH
Photo-Fenton
H_2O_2 decomposition

ABSTRACT

CuO_x-doped α-FeOOH (CuO_x–FeOOH) nanorods were synthesized by controlling the reaction between ferrous sulfate, cupric sulfate and sodium borohydride at ambient atmosphere. The resulting materials were characterized by transmission electron microscopy, X-ray powder diffraction, Fourier transform infrared spectroscopy, and X-ray photoelectron spectroscopy. CuO_x–FeOOH was mainly composed of α-FeOOH and CuO_x (CuO and Cu_2O). The catalyst was found to be highly effective for the degradation of endocrine disruptors, including dimethyl phthalate, 2,4-dichlorophenoxyacetic acid, and 2,4-dichlorophenol in the presence of H_2O_2 and UVA at neutral pH. By the total organic carbon and GC–MS analysis, the degradation process of DMP was shown to proceed with the cleavage of C–O bond in ester linkages and the phenyl ring opening into organic acids and CO_2. The studies of •OH formation and cyclic voltammetry revealed that the H_2O_2 was decomposed into •OH or O_2 by the promotion of metal oxide. The obtained results showed that the synergistic effect between CuO_x and α-FeOOH markedly enhanced the H_2O_2 decomposition into •OH in CuO_x–FeOOH suspension, causing the higher catalytic reactivity. A possible reaction mechanism was proposed.

1. Introduction

Endocrine disruptors (EDs) such as phthalates from domestic, agricultural and industrial sources have been widely released directly or indirectly to the aquatic environment [1]. EDs could alter endocrine functions and disrupt growth, development, and reproduction by interfering with the production of the endocrine system [2], which has become an important problem to environmental pollution, especially to drinking water safety. Therefore, removal and degradation of EDs from the environment has been an object of public concern.

Advanced oxidation processes such as photocatalytic oxidation, catalytic ozonation, and Fenton oxidation have gained popularity for effective organic destruction from wastewater [3], among which the Fenton reaction has attracted great attention due to its formation of highly potent chemical species, •OH, for non-selective oxidation [4,5]. However, the application of homogeneous Fenton reaction is limited by the narrow working pH range (<4), separation and recovery of the iron species [6]. Since many types of wastewater, such as municipal wastewater, usually have pH higher than 4, the pH has to be adjusted twice during homogeneous Fenton reactions, first to an acidic pH < 4 to carry out the Fenton pretreatment and then back to a neutral pH for final effluent discharge or subsequent bio-treatment [7]. To overcome these drawbacks and extend the working pH range, some efforts have been made to develop heterogeneous Fenton systems [8,9].

Recently, several copper- and iron-based heterogeneous Fenton-like systems have been reported [9–13], which exhibited high activity in degradation of organic pollutants. However, few studies were conducted to investigate the catalytic activity of a nanoscale bimetallic catalyst consisting of Cu and Fe in degrading EDs via photo-Fenton reaction. Moreover, in the previous works [13,14], the decomposition rate of H_2O_2 was usually a versatile indicator for the activity of different Fenton catalysts. It is very necessary to verify the veracity about the estimation.

In this paper, CuO_x–FeOOH was prepared by controlling the reaction between ferrous sulfate, cupric sulfate and sodium borohydride at ambient atmosphere. CuO_x–FeOOH was found to be highly effective for the degradation of endocrine disruptors at neutral pH when it was used as a heterogeneous Fenton catalyst. Furthermore, it was verified that the H_2O_2 decomposition and the catalytic activity were not correlative on the basis of all information obtained under different experimental conditions. The reaction mechanism of CuO_x–FeOOH was proposed.

* Corresponding authors. Tel.: +86 10 62849628; fax: +86 10 62923541.
E-mail addresses: huchun@rcees.ac.cn, (C. Hu)., jhqu@rcees.ac.cn, (J. Qu).

0926-3373/$ – see front matter © 2008 Published by Elsevier B.V.
doi:10.1016/j.apcatb.2008.08.022

2. Experimental

2.1. Materials and reagents

Ferrous sulfate heptahydrate, cupric sulfate pentahydrate, sodium borohydride, H_2O_2 (30%, w/w), dimethyl phthalate (DMP), 2,4-dichlorophenol (2,4-DCP), 2,4-dichlorophenoxyacetic acid (2,4-D) and dimethyl sulfoxide (DMSO) were analytical grade and obtained from the Yili Company. All other chemicals were analytical grade. Deionized and doubly distilled water was used throughout this study. The solution pH was adjusted by a diluted aqueous solution of NaOH or HCl.

2.2. Preparation of catalysts

CuO_x–FeOOH was synthesized by the reaction between ferrous sulfate, cupric sulfate and sodium borohydride in a 250-mL three-necked round-bottle flask. In a typical procedure, 2.78 g of $FeSO_4{\cdot}7H_2O$ and 0.85 g of $NaBH_4$ were dissolved in 100 and 50 mL deoxygenated water, respectively. The resulting ferrous sulfate solution was dropped into the flask charged with $NaBH_4$ solution in 25 min under N_2 atmosphere. Then 0.25 g of $CuSO_4{\cdot}5H_2O$ were dissolved in 10 mL deoxygenated water and added into the mixture above. The flask was vigorously stirred during the addition to avoid aggregation of the resultant particles. The black precipitates were centrifugated, washed with water for three times and finally dried at 70 °C for 10 h under ambient conditions.

As a comparison, copper oxide was also prepared by repeating the same reaction procedure described above and was denoted by CuO_x.

2.3. Characterization

TEM images of the catalyst were examined using a TEM Hitachi H-7500. The X-ray powder diffraction (XRD) patterns of the catalysts were recorded on a Scintag-XDS-2000 diffractometer with Cu Kα radiation (λ = 1.54059 Å). The infrared spectra of different samples supported on KBr pellets were recorded on a Fourier transform infrared (FT-IR) spectrophotometer (Nicolet 5700). The X-ray photoelectron spectroscopy (XPS) data were taken on an AXIS-Ultra instrument from Kratos using monochromatic Al Kα radiation (225 W, 15 mA, 15 kV) and low-energy electron flooding for charge compensation. To compensate for surface charge effects, the binding energies were calibrated using the C 1s hydrocarbon peak at 284.80 eV. The Cu concentration in the bulk of CuO_x–FeOOH was measured by flames atomic absorption spectrometry (AA-6300, Shimadzu) analysis (FAAS).

2.4. Procedures and analyses

The light source was a 300-W high-pressure mercury lamp fixed inside a cylindrical Pyrex flask, which was surrounded by a circulating water jacket to cool the lamp. The exterior of the cylindrical Pyrex flask was wrapped by tinfoil, leaving just a small window (3.5 cm × 1.5 cm) at the side face. The light was then focused onto a 100 mL glass reaction vessel. The average light intensity was 10 mW cm^{-2} (λ_{max} = 365 nm). To effectively suspend the catalyst, compressed air was bubbled from the bottom of the reactor. The reaction temperature was maintained at 25 °C.

In a typical experiment, 20 mg of catalyst were dispersed in 50 mL DMP solution (40 mg/L, pH 6.7). After the addition of H_2O_2 (5 mM) and UVA irradiation, at given time intervals, 0.5 mL samples were withdrawn and filtered through a millipore filter (pore size 0.45 μm). The filtrates were analyzed by a high-performance liquid chromatograph (HPLC, Hitachi L-2130) with an Xterra MS C18 column. 50% acetonitrite with 50% water mobile phase was used. Determination of hydroxyl radicals was performed with a photometric method [15,16] and the concentration of H_2O_2 was determined by $KMnO_4$ titration [17]. The cyclic voltammetry performance of CuO_x and CuO_x–FeOOH film electrode were investigated in a 0.1 M Na_2SO_4 solution with different H_2O_2 concentrations under UVA irradiation. The photo-electrocatalytic reaction employed a basic electrochemical system (Princeton Applied Research) connected with a counter-electrode (Pt wire, 70 mm in length with a 0.4 mm diameter), a working electrode (CuO_x or CuO_x–FeOOH film, active area of 6 cm^2), and a reference electrode (a saturated calomel electrode (SCE)). 0.1 M Na_2SO_4 solution was used as electrolyte solution.

The total organic carbon (TOC) of the solution was analyzed with a Phoenix 8000 TOC analyzer. GC–MS analysis was carried out on an Agilent 6890GC/5973MSD with a DB-5 MS capillary column. Sample for GC–MS analysis was prepared as follows: in the experiment, 20 mg of catalyst were dispersed in 50 mL DMP

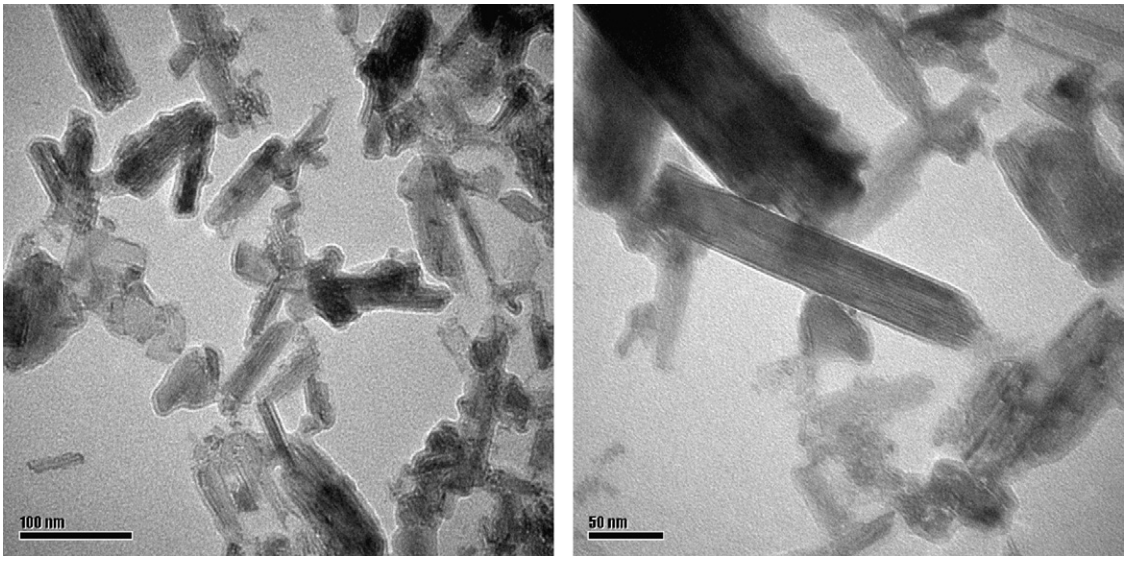

Fig. 1. TEM images of the as-prepared CuO_x–FeOOH.

solution (20 mg/L, pH 6.7). After the addition of H_2O_2 (5 mM) and UVA irradiation, at 3 and 30 min reaction time, the samples were withdrawn and filtered to remove CuO_x–FeOOH. The solutions were evaporated by freeze-dried method. The residues were trimethylsilylated with 0.2 mL of anhydrous pyridine, 0.1 mL of hexamethyldisilazane, and 0.05 mL of chlorotrimethylsilane at room temperature.

3. Results and discussion

3.1. Characterization of catalysts

Fig. 1 shows the TEM images of CuO_x–FeOOH. Obviously, the material was mainly rod-like nanoparticles. The size of individual particles ranged from 50 to 100 nm, while a few particles may be as large as 200–250 nm. Fig. 2 shows the XRD patterns of α-FeOOH, CuO_x–FeOOH and CuO_x. CuO_x–FeOOH exhibited similar peaks of XRD patterns with α-FeOOH (curve a), while almost no diffraction peak for the crystalline phases of copper oxides was observed (curve b). This was presumably due to the low content, smaller particle sizes and high dispersion of CuO_x in the particle. The XRD patterns of the bulk CuO_x (curve c) were readily indexed to a cubic phase Cu_2O (JCPDS No. 05-0667). Also, different catalysts were characterized with FT-IR. As shown in Fig. 3, for CuO_x–FeOOH (curve a), the two peaks at 3440 and 3170 cm^{-1} were assigned to the O–H stretching of α-FeOOH, while the two absorption peaks at around 887 and 790 cm^{-1} could be attributed to hydroxyl deformation and stretching of α-FeOOH [18]. The bending vibration of adsorbed water was observed at 1645–1613 cm^{-1} [19]. The characteristic peaks at 1384 and 620 cm^{-1} indicated the existence of Cu_2O [20], while the peak at 475 cm^{-1} might be assigned to the vibrations of Cu(II)-O, indicating the existence of polycrystalline CuO [21]. The FT-IR spectrum of CuO_x (curve c) confirmed the existence of Cu_2O and polycrystalline CuO in the structure of CuO_x. Moreover, the color of CuO_x is black, which suggests that polycrystalline CuO is predominant. Furthermore, the metallic state of Cu and Fe in CuO_x–FeOOH was characterized by XPS. In the Cu $2p_{3/2}$ core level XPS spectra, the peaks corresponding to the Cu $2p_{3/2}$ were observed at 932.7, and 934.7 eV, for Cu_2O and CuO, respectively (Fig. 4a) [22]. The peaks at 711, 719, and 725 eV that represented the binding energies of Fe $2p_{3/2}$, shake-up satellite Fe $2p_{3/2}$, and Fe $2p_{1/2}$, respectively were shown in Fig. 4b, indicating the existence of Fe_2O_3 or FeOOH [23]. According to XRD and FT-IR analysis, the iron oxide of CuO_x–FeOOH was mainly composed of α-FeOOH. By FAAS analysis, the Cu concentration in the bulk of CuO_x–FeOOH was 5.58 wt%, which was more than the Cu surface concentration 4.67 wt% from the result of XPS. The results indicated that more Cu existed in the bulk of α-FeOOH.

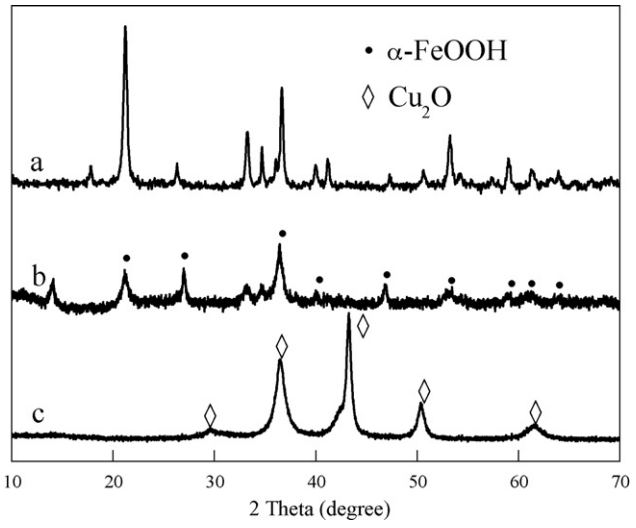

Fig. 2. XRD patterns of (a) α-FeOOH, (b) CuO_x–FeOOH, and (c) CuO_x.

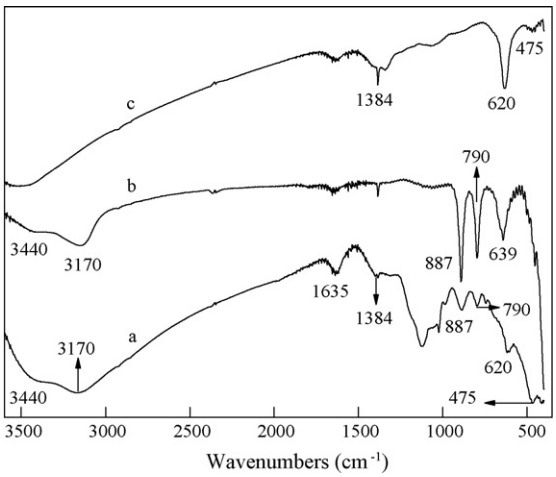

Fig. 3. FT-IR spectra of (a) CuO_x–FeOOH, (b) α-FeOOH, and (c) CuO_x.

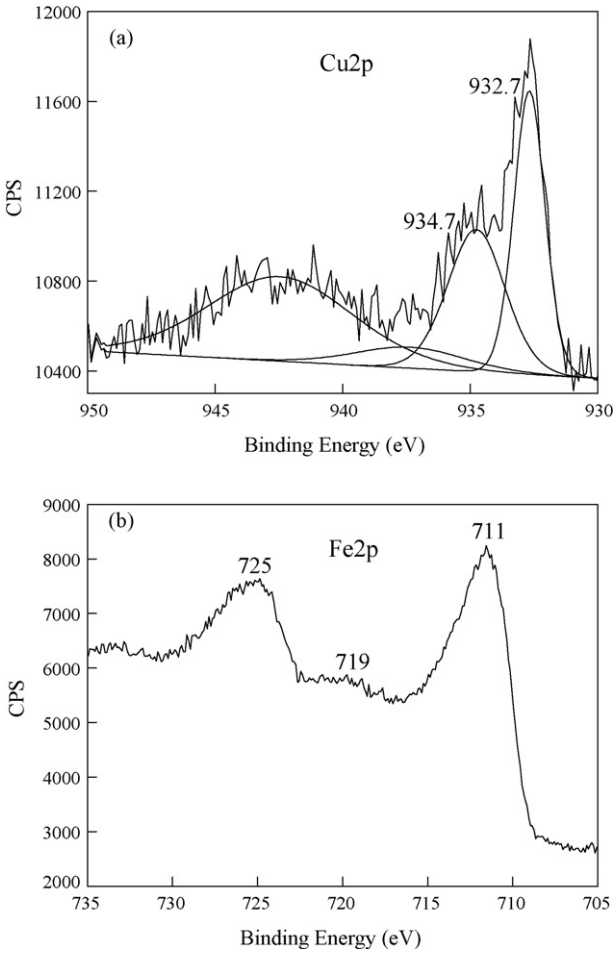

Fig. 4. XPS spectrum of CuO_x–FeOOH: (a) Cu 2p and (b) Fe 2p.

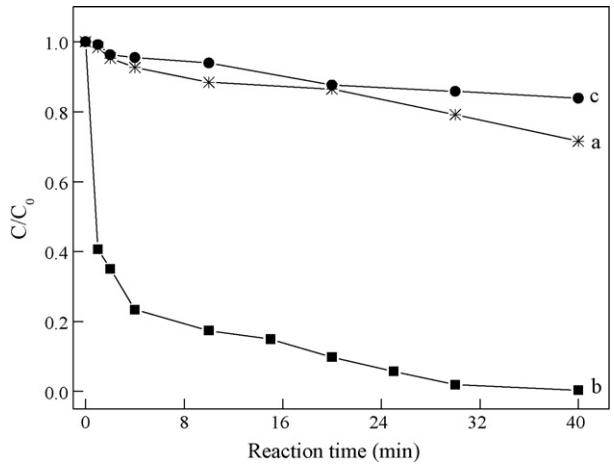

Fig. 5. The activity of as-prepared CuO_x–FeOOH with different ratio of copper to iron for the degradation of DMP in the presence of H_2O_2 and UVA: (a) 1:30, (b) 1:10, and (c) 1:5 (experimental conditions: 50 mL, 40 mg/L DMP, pH 6.7, 5 mM H_2O_2, addition of catalyst, 0.4 g/L).

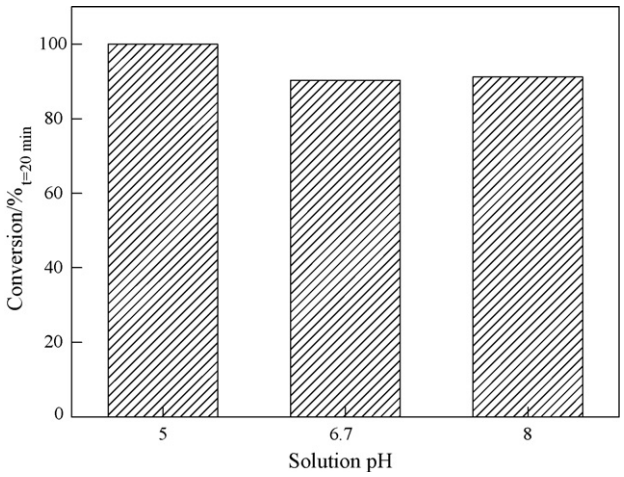

Fig. 7. Effect of pH on the activity of CuO_x–FeOOH in the presence of H_2O_2 and UVA (50 mL 40 mg/L DMP, pH 6.7, 5 mM H_2O_2, addition of catalyst, 0.4 g/L).

3.2. Degradation of endocrine disruptors

3.2.1. The optimal amount of doped CuO_x

By FAAS analysis, the actual chemical compositions of Cu in CuO_x–FeOOH with different ratio of copper to iron (1:30, 1:10, 1:5) in the starting material were 2.18, 5.58 and 4.36 wt%. The activities of these samples in the presence of H_2O_2 and UVA were shown in Fig. 5. The sample with the ratio of Cu to Fe 1:10 exhibited the highest efficiency for the degradation of DMP, which was used for all the experiments unless otherwise specified.

3.2.2. Performance of different catalysts

The activities of different catalysts were evaluated by the degradation of DMP at neutral pH under different conditions. As shown in Fig. 6, CuO_x–FeOOH did not exhibit any activity for the degradation of DMP either in the dark or under UVA irradiation in the absence of H_2O_2 (data not shown). However, complete fast abatement of 20 mg/L DMP was observed within 5 min (curve a) in aqueous CuO_x–FeOOH suspension with H_2O_2 and UVA. At the same time, about 40% of DMP was degraded in the presence of CuO_x–FeOOH and H_2O_2 in the dark (curve b). Some degree of DMP degradation occurred in homogeneous Fe^{3+} and Cu^{2+} solution with H_2O_2 and UVA (ca. 25%, curve c), while neither α-FeOOH nor CuO_x showed any activity in the degradation of DMP in the H_2O_2/UVA system (curves d and e). These results indicated that CuO_x–FeOOH was an excellent heterogeneous Fenton catalyst and the introduction of copper oxides played an important role in the enhancement of the catalyst activity. Furthermore, the degradation of DMP was performed in the CuO_x–FeOOH/H_2O_2/UVA system with varying initial pHs (Fig. 7). Clearly, the catalyst showed highly catalytic activity from acidic to alkaline (pH 5–8) and more than 90% degradation of DMP was achieved within 20 min of reaction in all cases. As shown in Fig. 8, CuO_x–FeOOH exhibited highly catalytic activity for the degradation of other endocrine disruptors. Both 2,4-D and 2,4-DCP were degraded efficiently over the catalyst in the H_2O_2/UVA system as DMP. It was found that the TOC removal ratio followed the order 2,4-D > 2,4-DCP > DMP.

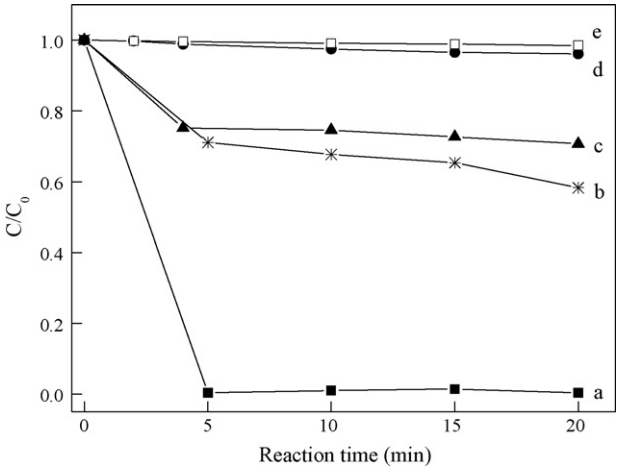

Fig. 6. Catalytic degradation of DMP (20 mg/L, 50 mL) under different conditions: (a) CuO_x–FeOOH + H_2O_2 + UVA, (b) CuO_x–FeOOH + H_2O_2, (c) Cu^{2+}, Fe^{3+} + H_2O_2 + UVA, (d) α-FeOOH + H_2O_2 + UVA, (e) CuO_x + H_2O_2 + UVA (pH 6.7, H_2O_2: 5 mM, catalyst: 0.4 g/L).

3.2.3. Formation of intermediates

The process of DMP degradation was further examined with GC–MS by determining the intermediates after DMP was degraded for 3 and 30 min (Tables 1 and 2). All the identified compounds were unequivocally identified using the NIST98 library database with fit values higher than 90%. The main products included phthalic acid and aliphatic acids, succinic acid, maleic acid, malonate and 2-hydroxy-propanoic acid at 3 min of irradiation when about 70% DMP was degraded. Further 30 min of irradiation, most of intermediates, such as phthalic acid, succinic acid and maleic acid disappeared, while malonate, 2-hydroxy-propanoic acid still present. DMP degradation proceeded by the cleavage of C–O bond in ester linkages and the formation of methanol and phthalic acid. Subsequently, the phenyl ring was opened into organic acids. The final step involved was the further oxidization of the organic acids to produce carbon dioxide and water.

3.3. Decomposition of H_2O_2 and the catalytic activity

Zhao and co-workers reported that H_2O_2 decomposition proceeded synchronously with the degradation of organic pollutants during heterogeneous photo-Fenton processes [8,24]. Therefore, H_2O_2 decomposition was used directly to evaluate the performance of different Fenton catalysts [14,25]. However, no significant correlation was found between H_2O_2 decomposition and the catalyst's activity for different Fenton processes in our study. The results of H_2O_2 decomposition under different conditions were shown in Fig. 9. Compared with Fig. 6, α-FeOOH

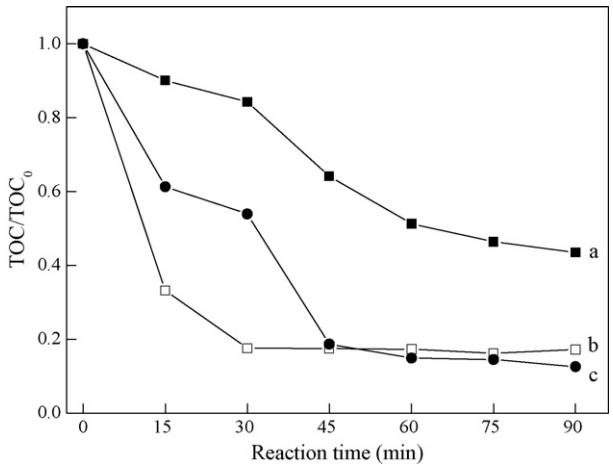

Fig. 8. TOC changes of different organic compounds (40 mg/L, 50 mL, pH 6.7) over CuO_x–FeOOH in the presence of H_2O_2 (5 mM) and UVA: (a) DMP, (b) 2,4-D and (c) 2,4-DCP.

showed the lowest activity for H_2O_2 decomposition and the DMP degradation under UVA irradiation (curve a). However, the decomposition rate of H_2O_2 was much higher over CuO_x than that over CuO_x–FeOOH under UVA irradiation or not. About 62% and 96% of H_2O_2 was decomposed in CuO_x suspension either in the dark (curve c) or under UVA irradiation (curve e), while only 21% and 53% of H_2O_2 were decomposed in CuO_x–FeOOH suspension under the same conditions (curves b and d). The results did not agree with those of the degradation of DMP under the same conditions. CuO_x exhibited the highest activity for H_2O_2 decomposition, oppositely, it did not show any activity for the degradation of DMP. CuO_x–FeOOH exhibited the highest catalytic activity toward DMP degradation. As shown in Fig. 10, the generation of •OH under different conditions was determined by the reaction of •OH with DMSO. Obviously, there was almost no •OH formation in aqueous CuO_x dispersions (curves a and b) with the fast decomposition of H_2O_2 under UVA or not, indicating CuO_x was non-effective for the DMP degradation. While in other catalyst suspensions under otherwise identical conditions, the quantities of formed •OH increased with the reaction time. Especially, in CuO_x–FeOOH/H_2O_2/UVA system, 54 μM of •OH was formed within 2 min, and the concentration of •OH rapidly decreased and reached a certain value. The result indicated that the reaction system had a very high efficiency at the initial stage, which was shown in Fig. 6, the DMP completely disappeared within 5 min. Therefore, the decomposition of H_2O_2 could not always exactly reflect the catalytic efficiency, which depends on the formation of active oxygen species. Clearly, the intermediates from H_2O_2 decomposition were different between CuO_x suspension and CuO_x–FeOOH suspension. To ascertain the conjecture, the cyclic voltammetry behaviors of CuO_x and CuO_x–FeOOH film electrodes were investigated in a 0.1 M Na_2SO_4 solution. As shown in Fig. 11, the current densities approximated to zero (curves a–c) in both H_2O_2/UVA and CuO_x–FeOOH film electrode/H_2O_2/UVA systems. The current densities increased to some extent with the applied potential from 0.1 to 1.0 V (curve d) in CuO_x–FeOOH film electrode/H_2O_2 system. In contrast, in the CuO_x film electrode/H_2O_2 system, the current densities increased with the increase of the applied potential from 0.1 to 1.0 V (curve e). Under UVA irradiation, the current densities were greatly enhanced (curve f), and became much more strong with increasing H_2O_2 concentration (curve g). In the above three conditions, the current densities increased largely with increasing the potential over 0.4 V, and a shoulder was observed at around 0.7 V (curves b and c). The electron potential of O_2/H_2O_2 was 0.69 V (vs. SCE), while the electrode potentials of Cu^{2+}/Cu^0 and Cu^{2+}/Cu^+ were 0.34 and 0.17 V (vs. SCE), respectively. Therefore, the peak should be attributed to the evolution of oxygen from the decomposition of H_2O_2. The studies of the cyclic voltammetry verified that CuO_x predominantly decomposed H_2O_2 into O_2 and H_2O.

Table 1
Identified products of DMP degradation detected by GC–MS after 3-min reaction in CuO_x–FeOOH/H_2O_2/UVA system

Retention time (min)	Product	Molecular structure
8.342	2-Hydroxy-propanoic acid	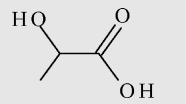
8.553	3-Hydroxy-butyric acid	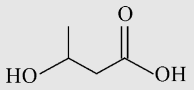
9.325	Hydroxyacetic acid	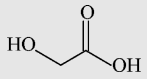
10.900	Glycol	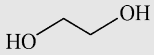
16.767	2-Ethyl-hexanoic acid	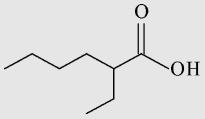
22.023	Malonate	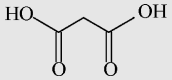
28.222	Glycerin	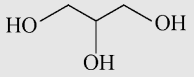
29.757	Maleic acid	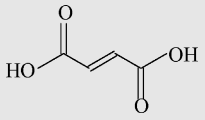
30.517	Succinic acid	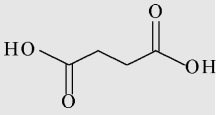
36.738	Dimethyl phthalate	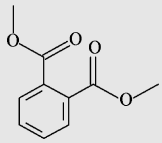
45.604	Phthalic acid	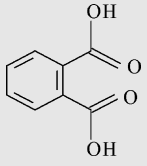

Table 2
Identified products of DMP degradation detected by GC–MS after 30-min reaction in CuO_x–FeOOH/H_2O_2/UVA system

Retention time (min)	Product	Molecular structure
8.362	2-Hydroxy-propanoic acid	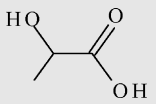
13.808	Glycol	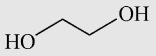
16.777	2-Ethyl-hexanoic acid	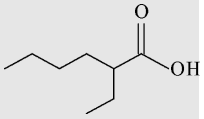
22.023	Malonate	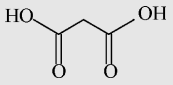
28.222	Glycerin	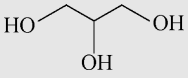

3.4. Mechanism discussion

The H_2O_2 decomposition promoted by transition metal oxide has been proposed in the literature to take place by two possible reaction pathways: (i) via a surface oxygen vacancies (V_{surf}) mechanism and (ii) via radical reactions. In the first mechanism (reactions (1) and (2)), oxygen vacancies on the oxide surface participate in the reaction by activating H_2O_2 molecules to produce O_2. This mechanism has been proposed for different oxides, such as perovskites [26].

$$V_{surf} + H_2O_2 \rightarrow V{-}O_{surf} + H_2O \quad (1)$$

$$V{-}O_{surf} + H_2O_2 \rightarrow V_{surf} + O_2 + H_2O \quad (2)$$

In aqueous CuO_x suspension, the decomposition of H_2O_2 was not significantly enhanced in the presence of radical scavengers

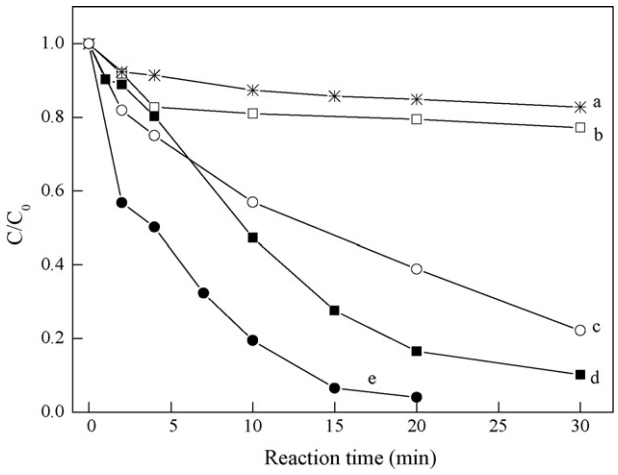

Fig. 9. H_2O_2 decomposition under different conditions: (a) α-FeOOH + H_2O_2 + UVA, (b) CuO_x–FeOOH + H_2O_2, (c) CuO_x + H_2O_2, (d) CuO_x–FeOOH + H_2O_2 + UVA and (e) CuO_x + H_2O_2 + UVA (DMP: 40 mg/L, 50 mL, pH 6.7, H_2O_2: 5 mM, catalyst: 0.4 g/L).

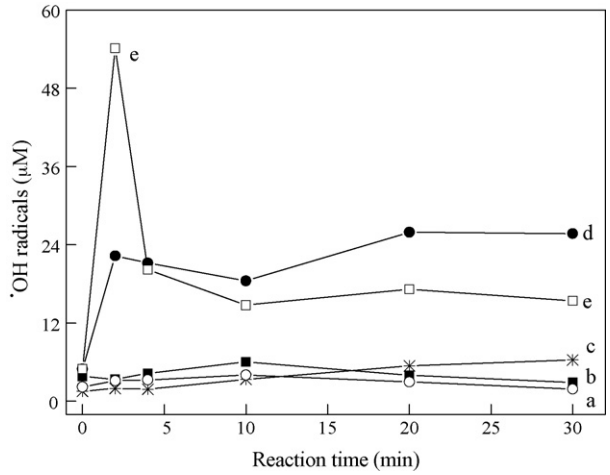

Fig. 10. Generation of hydroxyl radicals over different catalysts at neutral pH: (a) CuO_x + H_2O_2, (b) CuO_x + H_2O_2 + UVA, (c) α-FeOOH + H_2O_2 + UVA, (d) CuO_x–FeOOH + H_2O_2 and (e) CuO_x–FeOOH + H_2O_2 + UVA (H_2O_2: 5 mM, catalyst: 0.4 g/L).

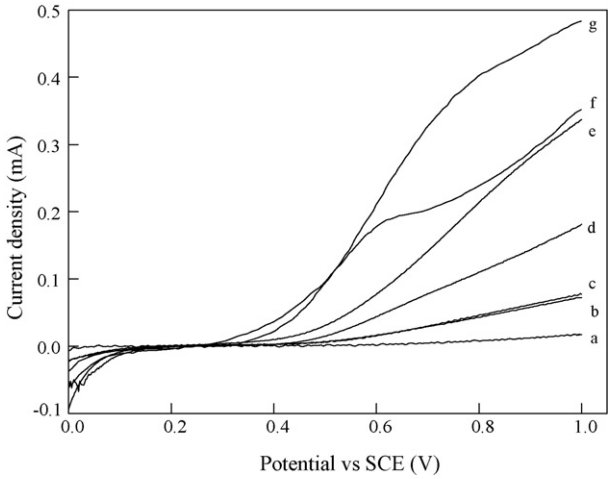

Fig. 11. Cyclic voltammetry scans with CuO_x and CuO_x–FeOOH electrodes in a 0.1 M Na_2SO_4 electrolyte with various concentrations of H_2O_2 at neutral pH: (a) 5 mM H_2O_2 + UVA, (b) CuO_x–FeOOH + 5 mM H_2O_2 + UVA, (c) CuO_x–FeOOH + 10 mM H_2O_2 + UVA, (d) CuO_x–FeOOH + 5 mM H_2O_2 + dark, (e) CuO_x + 5 mM H_2O_2 + dark, (f) CuO_x + 5 mM H_2O_2 + UVA and (g) CuO_x + 10 mM H_2O_2 + UVA.

tert-butanol, DMP and DMSO, which have the reaction rate constant 5×10^8, 4×10^9 and 7×10^9 M^{-1} s^{-1} with •OH [27,28], respectively (Fig. 12). Moreover, no •OH formation was determined with the decomposition of H_2O_2. These results suggested that the reaction over CuO_x did not proceed via a radical mechanism. The study of the •OH formation verified that the decomposition of H_2O_2 catalyzed by CuO_x–FeOOH underwent radical reactions. Although the mechanism of radical generation is not clear, a simple proposal is the initiation by the reaction of H_2O_2 with Cu^+ and reduced Fe^{2+} surface species, according to Haber-Weiss mechanism:

$$\equiv Fe^{3+} + h\nu \rightarrow \equiv Fe^{2+} \quad (3)$$

$$\equiv Cu^{+} + \equiv Fe^{3+} \rightarrow \equiv Cu^{2+} + \equiv Fe^{2+} \quad (4)$$

$$\equiv Fe^{2+} + H_2O_2 \rightarrow \equiv Fe^{3+} + {}^{\bullet}OH + OH^{-} \quad (5)$$

$$\equiv Cu^{+} + H_2O_2 \rightarrow \equiv Cu^{2+} + {}^{\bullet}OH + OH^{-} \quad (6)$$

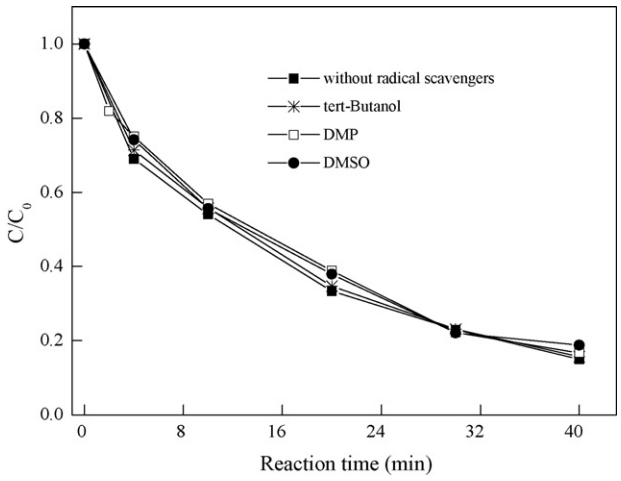

Fig. 12. Effect of radical scavengers on the H_2O_2 decomposition over CuO_x in the presence of H_2O_2 and UVA (radical scavengers: 50 mL 40 mg/L, pH 6.7, 5 mM H_2O_2, addition of catalyst, 0.4 g/L).

Since the reduction of Fe^{3+} by Cu^+ (reaction (4)) is thermodynamically favorable as shown by the following equations:

$$Cu^{2+} + e^- \rightarrow Cu^+, \quad E^0 = 0.17\,V \tag{7}$$

$$Fe^{3+} + e^- \rightarrow Fe^{2+}, \quad E^0 = 0.77\,V \tag{8}$$

Compared with α-FeOOH, the introduction of CuO_x not only led to the more Fe^{2+} species formation on the surface of CuO_x–FeOOH, enhancing reaction (4), but also generated $^\bullet$OH by reaction (5). In addition, Cu^+ could be generated from the following reactions:

$$^\bullet OH + H_2O_2 \rightarrow HO_2^\bullet + H_2O \tag{9}$$

$$\equiv Cu^{2+} + HO_2^\bullet \rightarrow \equiv Cu^+ + O_2 + H^+ \tag{10}$$

$$\equiv Cu^{2+} + h\nu \rightarrow \equiv Cu^+ \tag{11}$$

Thus, by the role of both Fe^{3+}/Fe^{2+} pair and Cu^{2+}/Cu^+ pair, the interfacial electron transfer was greatly enhanced in CuO_x–FeOOH, and H_2O_2 was efficiently decomposed into $^\bullet$OH radicals. In addition, based on the above reactions, by UVA irradiation, Fe^{3+} and Cu^{2+} could be transformed into Fe^{2+} and Cu^+, which are active components for the $^\bullet$OH formation from H_2O_2. Also, the cycle of Fe^{3+}/Fe^{2+} and Cu^{2+}/Cu^+ pair were enhanced by UVA irradiation. Therefore, the UV irradiation significantly increased the activity of CuO_x–FeOOH from Fig. 6. All the results suggested that $^\bullet$OH formation was rather a better indicator for Fenton catalyst's activity than H_2O_2 decomposition. The mechanism presented need to be further clarified.

4. Conclusions

CuO_x-doped α-FeOOH (CuO_x–FeOOH) produced a highly efficient heterogeneous photo-Fenton catalyst for the degradation of endocrine disruptors. No significant correlation was found between H_2O_2 decomposition and the catalyst's activity for different Fenton processes. The studies of $^\bullet$OH formation and cyclic voltammetry revealed that the H_2O_2 was decomposed into $^\bullet$OH or O_2 by the promotion of metal oxide. The synergistic effect between CuO_x and α-FeOOH markedly enhanced the H_2O_2 decomposition into $^\bullet$OH in CuO_x–FeOOH suspension, causing the higher catalytic reactivity.

Acknowledgments

This work was supported by the National Natural Science Foundation of China (No. 50778169, 50621804) and the National 863 Project of China (Grant No. 2006AA06Z304).

References

[1] B.L.L. Tan, D.W. Hawker, J.F. Muller, F.D.L. Leusch, L.A. Tremblay, H.F. Chapman, Chemosphere 69 (2007) 644.
[2] C. Ooka, H. Yoshida, M. Horio, K. Suzuki, T. Hattori, Appl. Catal. B: Environ. 41 (2003) 313.
[3] R. Thiruvenkatachari, T.O. Kwon, J.C. Jun, S. Balaji, M. Matheswaran, I.S. Moon, J. Hazard. Mater. B 142 (2007) 308.
[4] Z. Ai, L. Lu, J. Li, J. Qiu, M. Wu, J. Phys. Chem. C 111 (2007) 4087.
[5] H. Liu, C. Wang, X. Li, X. Xuan, C. Jiang, H. Cui, Environ. Sci. Technol. 41 (2007) 2937.
[6] X. Lv, Y. Xu, K. Lv, G. Zhang, J. Photochem. Photobiol. A: Chem. 173 (2005) 121.
[7] S. Parra, I. Guasaquillo, O. Enea, E. Mielczarski, J. Mielczarki, P. Albers, L. Kiwi-Minsker, J. Kiwi, J. Phys. Chem. B 107 (2003) 7026.
[8] J. He, W. Ma, J. He, J. Zhao, J. Yu, Appl. Catal. B: Environ. 39 (2002) 211.
[9] H. Lim, J. Lee, S. Jin, J. Kim, J. Yoon, T. Hyeon, Chem. Commun. 4 (2006) 463.
[10] A.C.K. Yip, F.L.Y. Lam, X. Hu, Chem. Commun. 25 (2005) 3218.
[11] A.C.K. Yip, F.L.Y. Lam, X. Hu, Chem. Eng. Sci. 62 (2007) 5150.
[12] J.K. Kim, I.S. Metcalfe, Chemosphere 69 (2007) 689.
[13] P. Baldrian, V. Merhautova, J. Gabriel, F. Nerud, P. Stopka, M. Hruby, M.J. Benes, Appl. Catal. B: Environ. 66 (2006) 258.
[14] F.C.C. Moura, G.C. Oliveira, M.H. Araujo, R.M. Lago, Appl. Catal. A: Gen. 307 (2006) 195.
[15] C.F. Babbs, M.J. Gale, Anal. Biochem. 163 (1987) 67.
[16] M.G. Steiner, C.F. Babbs, Arch. Biochem. Biophys. 278 (1990) 478.
[17] N.V. Klassen, D. Marchington, H.C.E. McGowan, Anal. Chem. 66 (1994) 2921.
[18] H.D. Ruan, R.L. Frost, J.T. Kloprogge, L. Duong, Spectrochim. Acta Part A 58 (2002) 967.
[19] C. Hu, Y. Wang, H. Tang, Appl. Catal. B: Environ. 30 (2001) 277.
[20] H. Yang, J. Ouyang, A. Tang, Y. Xiao, X. Li, X. Dong, Y. Yu, Mater. Res. Bull. 41 (2006) 1310.
[21] A. Jagminas, J. Kuzmarskyt, G. Niaura, Appl. Surf. Sci. 201 (2002) 129.
[22] Y. Zhang, J. Tang, G. Wang, M. Zhang, X. Hu, J. Cryst. Growth 294 (2006) 278.
[23] X. Li, W. Zhang, Langmuir 22 (2006) 4638.
[24] M. Cheng, W. Ma, J. Li, Y. Huang, J. Zhao, Environ. Sci. Technol. 38 (2004) 1569.
[25] R.C.C. Costa, M.F.F. Lelis, L.C.A. Oliveria, J.D. Fabris, J.D. Ardisson, R.R.V.A. Rios, C.N. Silva, R.M. Lago, J. Hazard. Mater. B 129 (2006) 171.
[26] Y.N. Lee, R.M. Lago, J.L.G. Fierro, J. Gonzalez, Appl. Catal. A: Gen. 215 (2001) 245.
[27] J. Ma, N.J.D. Graham, Water Res. 34 (2000) 3822.
[28] W.R. Haag, C.C.D. Yao, Environ. Sci. Technol. 26 (1992) 1005.